

Article

Quasi-Static Compression Deformation and Energy Absorption Characteristics of Basalt Fiber-Containing Closed-Cell Aluminum Foam

Donghui Yang ^{1,†}, Zichen Zhang ^{1,†}, Xueguang Chen ^{1,*}, Xing Han ³, Tao Xu ¹, Xinglei Li ³, Jian Ding ^{1,*}, Haifeng Liu ³, Xingchuan Xia ^{1,*}, Yugang Gao ³, Yujiang Wang ^{2,*} and Yu Sun ³

¹ School of Material Science and Engineering, Hebei University of Technology, Tianjin 300401, China; 17596530308@163.com (D.Y.); zhangzc6666@163.com (Z.Z.); xu967777@163.com (T.X.)

² National Key Laboratory for Remanufacturing, Army Academy of Armored Forces, Beijing 100070, China

³ CITIC Dicastal Co., LTD., Qinhuangdao 066011, China; hanxing@dicastal.com (X.H.); 13229077022@163.com (X.L.); liuhaifeng@dicastal.com (H.L.); gaoyugang@dicastal.com (Y.G.); 18954133620@163.com (Y.S.)

* Correspondence: cxg@hebut.edu.cn (X.C.); djian0122@126.com (J.D.); xc_xia@hebut.edu.cn (X.X.); hitwyj@126.com (Y.W.); Tel.: +86-22-6020-2011 (X.X.); Fax: +86-22-6020-2011 (X.X.)

† These authors contributed equally to this work.

Received: 22 June 2020; Accepted: 5 July 2020; Published: 9 July 2020



Abstract: In this work, closed-cell aluminum foams with 4 wt.% contents of short-cut basalt fibers (BFs) were successfully prepared by using the modified melt-foaming method. The pore size of BF-containing aluminum foam and commercially pure aluminum foam was counted. The distribution of BF and its effect on the compressive properties of closed-cell aluminum foams were investigated. The results showed that the pore size of BF-containing aluminum foams was more uniform and smaller. BF mainly existed in three different forms: Some were totally embedded in the cell walls, some protruded from the cell walls, and others penetrated through the cells. Meanwhile, under the present condition, BF-containing aluminum foams possessed higher compressive strength and energy absorption characteristics than commercially pure aluminum foams, and the reasons were discussed.

Keywords: aluminum foam; melt foaming method; basalt fiber; compressive property

1. Introduction

Closed-cell aluminum foams are a class of novel structure materials with closed pores in pure aluminum or aluminum alloys [1]. Owing to its unique pore structure, closed-cell aluminum foam possesses ultra-low density, excellent sound-absorbing properties, vibration damping, electromagnetic shielding, and good energy absorption performance, which have made them widely used in transportation, construction, automobile fields, and so on [2–4]. Generally, excellent mechanical properties are needed to meet the requirement of structural materials. However, up until now, adjusting the relative density is most commonly applied to obtain higher mechanical properties, especially compression properties [5]. Besides, alloying and aluminum matrix syntactic foams (AMSFs) were used to optimize its compression performances. Huang et al. [6] studied the effect of Sc on the mechanical properties of aluminum foam, and found that minor Sc additions and subsequent proper heat treatment can dramatically improve the compressive strength of aluminum foams. Xia et al. [7,8] conducted a series of quasi-static compression tests on Mn-containing aluminum foams, and it was shown that Mn can significantly enhance the microhardness, compressive strength, energy absorption capacity, and seawater corrosion resistance of aluminum foam. Orbulov [9] studied the compression performance of aluminum foam reinforced by two kinds of hollow ceramic balls with different sizes

and found that smaller hollow ceramic balls can enormously boost the mechanical properties of aluminum foam. Zhang et al. [10] investigated the characteristics of multi-walled carbon nanotubes (MWCNTs)-reinforced closed-cell aluminum foam and discovered that MWCNTs can improve the yield strength, structural stiffness, and energy absorption of closed-cell aluminum foam. Li et al. [11] investigated the quasi-static and dynamic compressive properties of basalt scale-reinforced aluminum foam and spotted that basalt scale can improve the plastic crush stress, plateau stress, and energy absorption capacity of aluminum alloy foam. It can be seen that reinforcements can affect the mechanical properties of aluminum foam, while it is known that Sc and MWCNTs are expensive, resulting in increased production costs. The density of Mn is much higher than that of aluminum and its dispersion uniformity should be fully considered. AMSFs often have lower porosity, weakening the weight reduction effect of aluminum foam. Although basalt scale possesses lower manufacturing costs, high specific surface area, and good bond strength with aluminum alloy, the dynamic viscosity of granular materials and aluminum melt is too low to stabilize the liquid film for a long time, which will cause pore structural defects and further affect the mechanical properties of aluminum foams [12,13]. Recently, it was proven that, compared to particles or scales, short fiber is more effective in increasing melt viscosity and stabilizing foam due to its large aspect ratio [14]. Therefore, it is possible to obtain closed-cell aluminum foam with good structural stability and higher mechanical properties by selecting a suitable short fiber as the reinforcement.

Basalt fiber (BF) is a new type of high-performance material with a low density ($2.5\text{--}3.05\text{ g/cm}^3$) and wide operating temperature range (from 4 to 923 K). Besides, it possesses excellent thermal, electric, and acoustic insulation, radiation resistance, oxidation resistance, and mechanical properties (with Young's modulus of 78–110 GPa and tensile strength of 2.8–4.8 GPa). Meanwhile, it is environmentally friendly as the recycling of BF is much more efficient than other fibers [15,16]. Due to its unique properties and cost-effectiveness, researchers have recently focused on it, and BF–aluminum composites with better mechanical properties than other aluminum matrix composites have been developed [17–21]. It was reported that Al–Ca–Si and Al–Fe–Si–Mn intermetallic compounds formed at the A356 aluminum alloy matrix and basalt fiber interfaces, indicating that BF has good interfacial bonding with aluminum matrix [22]. Therefore, it is foreseeable that BF should be an ideal strengthening phase, which is expected to obtain lightweight, high-strength, environmentally friendly, and cost-effective composite aluminum foam. Hence, in this work, 4 wt.% BF and commercially pure aluminum were used as raw materials to prepare BF-containing closed-cell aluminum foam. The distribution of BF and its effects on the quasi-static compressive characteristics of BF-containing aluminum foam were studied.

2. Materials and Experimental

2.1. Specimens Preparation

In this work, the raw materials were commercially pure aluminum ingots (with a purity of 99.5%, Tianjin Lizhong alloy Group Co., Ltd., Tianjin, China), Ca particles (thickening agent, with diameters of 1–2.5 mm, Fuchen Technology Co., Ltd., Cangzhou, China), commercially pure magnesium block (thickening agent and wetting agent, with a purity of 99.5%, Tianjin Dongyi Magnesium Products Co., Ltd., Tianjin, China), TiH_2 powders (foaming agent, commercially pure, 300 ± 20 mesh, Beijing Xingrongyuan Technology Co., Ltd., Beijing, China), and commercial BF (with diameters of 7–15 μm , length of about 5 mm, 52–58 wt.% SiO_2 , 9–14 wt.% $\text{FeO}+\text{Fe}_2\text{O}_3$, 0.5–2.5 wt.% TiO_2 , 14–19 wt.% Al_2O_3 , 5–9 wt.% CaO , 3–6 wt.% MgO , Shijiazhuang Huabang mineral products Co., Ltd., Beijing, China). Detailed preparation processes were as follows: (1) Keeping BF at $773 \pm 5\text{ K}$ for 30 min at atmosphere in a heat treatment furnace, then cooling it to room temperature in the air; (2) melting a certain quantity of aluminum ingot (800–900 g) in a low-carbon-steel crucible to a fixed temperature of $1000 \pm 5\text{ K}$; (3) adding a 0.5 wt.% pure magnesium block into the melt and holding for 2 min, then stirring the melt with a speed of 500 r/min for 2 min; (4) pouring BF into the melt with an impeller stirring speed of 500 r/min for 5 min and holding for 20 min; (5) lowering the temperature to $953 \pm 5\text{ K}$,

then adding 2.5 wt.% Ca particles to the melt with an impeller stirring speed of 500 r/min for 8 min; (6) packaging 0.8 wt.% TiH₂ (heat-treated at 753 K for 30 min) with aluminum foil and putting it into the melt with an impeller stirring speed of 1200 r/min for 30 s; (7) holding the melt for 2 min and then cooling the melt in the air. For comparison, pure closed-cell aluminum foam (without BF) was prepared under coincident processing parameters.

2.2. Microstructure Observation and Theoretical Calculation

Representative metallographic preparation processes were applied to prepare specimens for metallographic characterization: Specimens were ground through successive grades of silicon carbide abrasive papers up to 2000 grit, polished using 0.25 μm diamond polishing paste, and then ultrasonically cleaned with alcohol and dried with cold flowing air in a fuming cupboard. Microstructures and distributions of BF in aluminum foams were examined by a scanning electron microscope (SEM, JSM-6510A, JEOL, Tokyo, Japan) equipped with an energy-dispersive X-ray spectrometer (EDS). Pore size was determined by the software calculation method: Grinding, painting, and re-polishing the specimens, and then a high-definition camera were used to obtain the image, and Image-Pro Plus 6.0 software (6.0, Media Cybernetics Inc., Rockville, MD, USA) was used to calculate the pore size [23]. An analytical balance (with a precision of 0.0001 g, Shanghai Pingxuan Scientific Instrument Co., Ltd., Shanghai, China) and caliper (with a precision of 0.05 mm, Shanghai Gaozhi Precision Instrument Co., Ltd., Shanghai, China) were used to measure the weights and accurate dimensions, respectively [1,8].

In the present work, porosities of aluminum foams were calculated by Equation (1) [24].

$$P_d = \left(1 - \frac{\rho^*}{\rho_s}\right) \times 100\% \quad (1)$$

where P_d is the measured porosity of aluminum foam, ρ^* is the overall density of aluminum foam, which is calculated from the weight and volume, and ρ_s is the density of the matrix material (2.7 g/cm³).

Energy absorption capacity, energy absorption efficiency, and ideal energy absorption efficiency were calculated by Equations (2)–(4), respectively [25–27].

$$W = \int_0^\varepsilon \sigma(\varepsilon) d\varepsilon \quad (2)$$

$$E = \frac{1}{\sigma} \int_0^\varepsilon \sigma(\varepsilon) d\varepsilon \quad (3)$$

$$I = \frac{1}{\sigma_{max}\varepsilon} \int_0^\varepsilon \sigma(\varepsilon) d\varepsilon \quad (4)$$

where W is the energy absorption capacity, E is the energy absorption efficiency, I is the ideal energy absorption efficiency, σ is the stress, ε is the strain, and σ_{max} is the maximum stress in the selected region of the stress–strain curve.

2.3. Mechanical Properties Test

Specimens for compression tests were prepared with dimensions of 25 × 25 × 25 mm³ (at least seven complete cells were included to minimize the size effect [28]) by using an electro-discharging machine. Quasi-static compression tests were performed by using a SUNS electron universal material testing machine, with a maximum load of 300 kN (according to China Standard GB/T7314-2005). All tests were conducted under displacement control with a constant speed of 1.5 mm/min (with the initial strain rate of 0.001/s) at room temperature. Vaseline was used to minimize the friction between specimens and plates. Load and displacement were recorded by a data acquisition unit and a personal computer. Engineering stress and strain were calculated from the recorded data. In order to

obtain the effect of BF on the compression process, one of the compressed surfaces of BF-containing aluminum foam specimens was polished, and the specimens were then compressed at a certain strain. Afterward, the polished sections were observed immediately by scanning electron microscopy without any further metallographic treatment. Three specimens with similar pore size and porosity for each kind of aluminum foam were compressed and average data were used in this paper.

3. Results

3.1. Structures of BF-Containing Aluminum Foam

Figure 1a shows a representative cross-section morphology of aluminum foam with a BF content of 4 wt.%. It can be seen that the pore structures are homogeneous, and the pores are spherical and isolated. Based on statistical results (Figure 1b), the pore diameter of BF-containing aluminum foam is mainly distributed in the range of 0.5–4.5 mm, and only about 5% of pores are larger than 3.5 mm. As for the pure aluminum foam, it is mainly distributed in the range of 0.5–6 mm and about 24% of pores are larger than 3.5 mm, meaning that BF can reduce the pore size and improve the homogeneity of the pores.

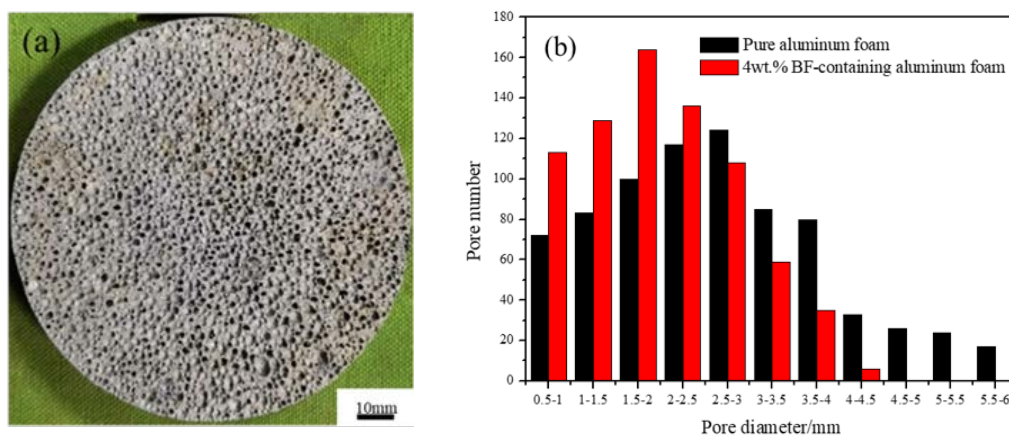


Figure 1. (a) Typical macrostructure; (b) pore size distribution.

3.2. Compressive Stress–Strain Curves

Figure 2 shows quasi-static compressive stress–strain curves of pure aluminum foam and BF-containing aluminum foam. It is clear that the stress–strain curves of BF-containing aluminum foams possess three stages, which is typical behavior of metallic foams: Elastic–plastic stage (I), where stress increases approximately linearly until reaching a local limit; stress plateau stage (II), where the buckling and plastic collapse of foam cells initiate and the stress is relatively constant over a large strain range; and densification stage (III), where the stress rises rapidly and the foam density quickly approaches its constitutive material [1,8]. It should be noted that the addition of BF substantially increases the compressive stresses of the foams. Meanwhile, the stress drop phenomenon appears on the stress–strain curves of BF-containing specimens, which is not observed on the pure aluminum foam. However, when the strain is greater than 0.1, no dentate stress fluctuations occur in the stress plateau stage, indicating that 4 wt.% BF can play a good reinforcing role during the compression process.

Yield strength, plateau stress, and densification strain are important parameters to characterize the mechanical properties of metallic foams, and are also widely used in the design and analysis of cellular solids [29]. In this paper, the first peak stress on the stress–strain curve is defined as yield strength [8], the extrapolation method is used to determine the densification strain [30], and the average stress within the strain range of 0.1 to 0.5 is defined as the plateau stress [31].

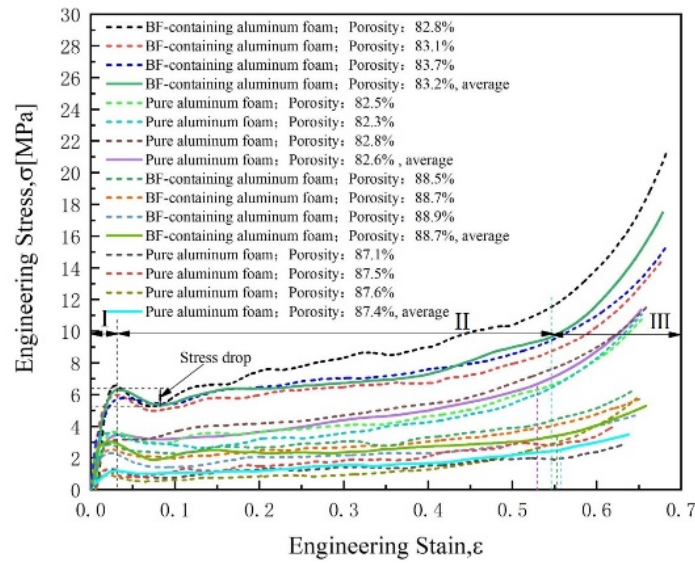


Figure 2. Stress–strain curves of two kinds of aluminum foams.

Figure 3 shows the statistical results of yield strength and plateau stress of two kinds of aluminum foams with different porosities. It indicates that BF-containing aluminum foams possess significantly higher yield strength and plateau stress than pure aluminum foams with similar pore structure. The plateau stress of BF-containing aluminum foams are 1.65 and 1.57 times as much as the pure aluminum foams, respectively. It can also be seen that the yield strength of two kinds of aluminum foams all decrease with the increase in porosity. When the porosity is about 83%, the yield strength of the BF-containing aluminum foam is about 6.18 MPa, which is 1.78 times the pure aluminum foam (3.48 MPa). Compared to the pure aluminum foam, when the porosity is close to 88%, the addition of BF has little effect on the densification strain (Figure 2). In addition, densification strains of BF-containing aluminum foams with different porosities are very similar, indicating that the densification strain of BF-containing aluminum foam is insensitive to porosity in the investigated porosity range.

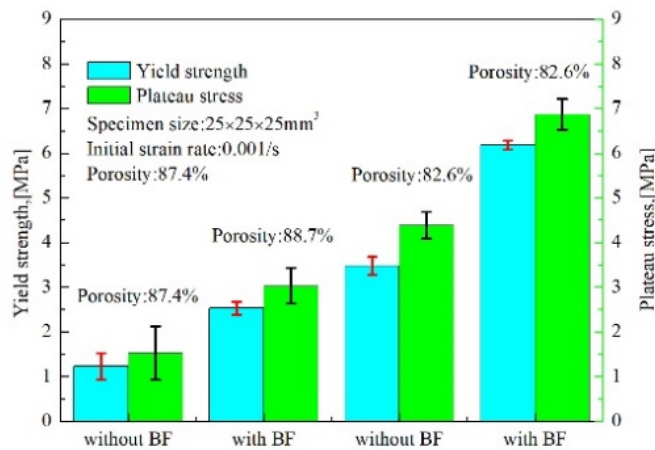


Figure 3. Yield strength and plateau stress of aluminum foams.

3.3. Energy Absorption Characteristics

Energy absorption characteristics are important for the application of metallic foams [5]. Therefore, energy absorption capacity (Equation (2)), energy absorption efficiency (Equation (3)), and ideal energy absorption efficiency (Equation (4)) were utilized to evaluate the energy absorption characteristics of BF-containing aluminum foams.

Figure 4 shows the energy absorption capacities of both pure aluminum foams and BF-containing aluminum foams. It is clear that energy absorption capacities increase with the increase in strain and decrease in porosity for all of the foams. Generally, energy absorption capacity is defined as the energy absorbed until densification strain during the compression test [1,8]. As shown in Figure 4, when the porosities of pure aluminum foam are 87.4% and 82.6%, the energy absorption capacities are 0.84 and 2.21 MJ/m³, respectively, while, for BF-containing aluminum foam, when the porosities are 88.7% and 83.2%, the energy absorption capacities are 1.39 and 3.65 MJ/m³, respectively. Meanwhile, it can be seen that the energy absorption capacity of BF-containing aluminum foam increases more significantly than that of pure aluminum foam under higher porosity, e.g., at the strain of 0.5, the W of BF-containing aluminum foam with a porosity of 88.7% is 74.58% higher than that of pure aluminum foam with a porosity of 87.4%. At the same strain of 0.5, the W of BF-containing aluminum foam with a porosity of 83.2% is 56.56% higher than that of pure aluminum foam with a porosity of 82.4%. All of this means that, compared to pure aluminum foams, BF-containing aluminum foams possess better energy absorption capacity regardless of the porosity.

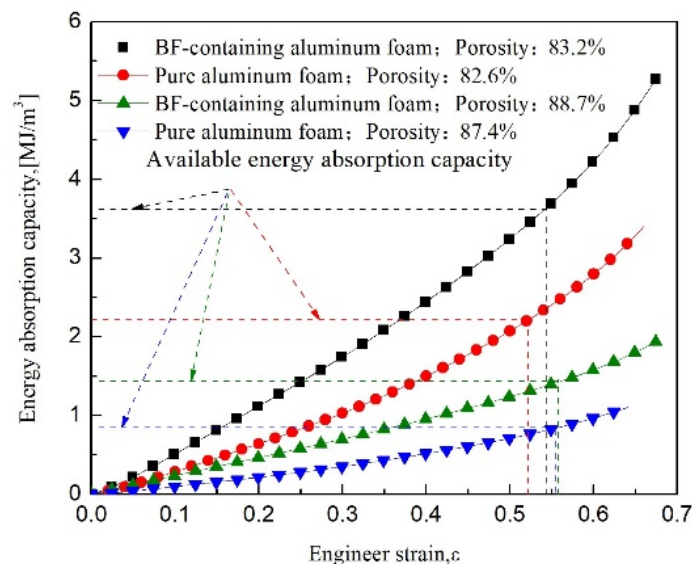


Figure 4. Energy absorption capacity of two kinds of aluminum foams.

Figure 5 shows the energy absorption efficiency of pure aluminum foams and BF-containing aluminum foams. It is clear that for both kinds of foams, energy absorption efficiency increases first and then decreases with the increasing strain. For pure aluminum foams, when porosities are 87.4% and 82.6%, the maximum energy absorption efficiencies are 0.336 and 0.341, respectively, while the corresponding maximum energy absorption efficiencies of BF-containing aluminum foams are about 0.418 and 0.384, meaning an increase of 24.4% and 12.61%, respectively. It should also be noted that when the porosity is close to 88%, the maximum energy absorption efficiency of pure aluminum foam instead decreases. However, the BF-containing aluminum foam specimen still has a higher energy absorption efficiency. This indicates that adding BF as reinforcement can greatly heighten the energy absorption efficiency of aluminum foam.

Figure 6 shows the ideal energy absorption efficiency of pure aluminum foams and BF-containing aluminum foams. As a general rule, an ideal energy absorption efficiency greater than 0.7 means cellular materials have good energy absorption capability [32]. In the present work, the stage with an ideal energy absorption efficiency exceeding 0.7 is defined as a high ideal energy absorption efficiency stage, and the average ideal energy absorption efficiency at this stage is used to compare the energy absorbing ability of both kinds of aluminum foam. From the view point of the high ideal energy absorption efficiency stage, the strain ranges of BF-containing aluminum foams are wider than those of pure aluminum foams with similar parameters, indicating BF-containing aluminum

foams can maintain high energy absorption efficiency for a long time. Meanwhile, it can be seen from Figure 6 that the average ideal energy absorption efficiency for pure aluminum foam is about 0.812 and 0.814, respectively, which are about 0.932 and 0.848, respectively, for BF-containing aluminum foams, meaning the addition of BF can obviously enhance the ideal energy absorption efficiency of aluminum foam.

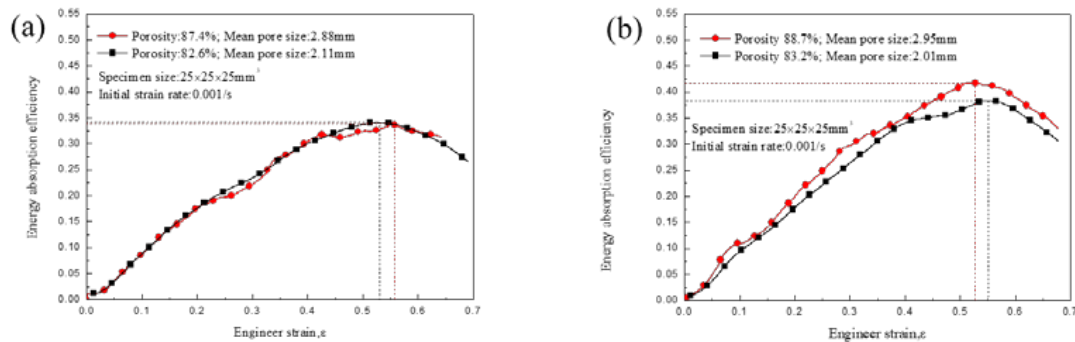


Figure 5. Energy absorption efficiency of aluminum foams: (a) Pure aluminum foam; (b) 4 wt.% basalt fiber (BF)-containing aluminum foam.

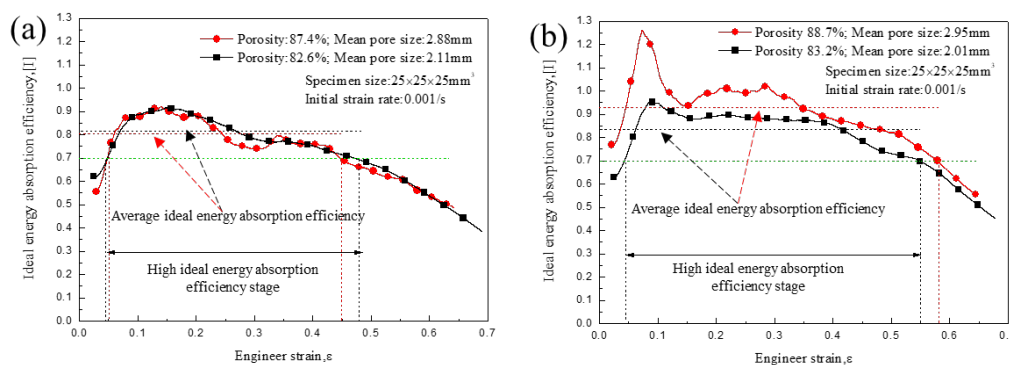


Figure 6. Ideal energy absorption efficiency of aluminum foams: (a) Pure aluminum foam; (b) 4 wt.% BF-containing aluminum foam.

4. Discussion

For short fibers-reinforced aluminum foams, the microstructure plays an important role in their compressive properties [33,34]. Therefore, the distribution of BF in aluminum foam was first observed to clarify the deformation mechanism of BF-containing aluminum foams. From Figure 7, it can be seen that there are mainly three distribution forms of BF in the foams. Some of them are entirely embedded in the cell walls (Figure 7a,b), which is similar to the reinforcements in bulk aluminum matrix composites [17–22], meaning the reinforcement effect of BF on aluminum foam is similar to those of BF-reinforced aluminum matrix composites. In addition, from Figure 7b, it can be observed that BF is randomly distributed in the cell walls. In addition, no defects along the interface of BF and the matrix can be found, indicating favorable interface bonding along the interfaces. As shown in Figure 7c, some BF partially protrudes from cell walls. It can also be seen from Figure 7d that a single BF penetrates through the cell. Meanwhile, rarely any BF is observed at the cell surface, meaning that all BF is located inside the cell walls, not at the interface. Furthermore, no bundles of BF in the cell walls and pores are observed, indicating that BF can completely disperse into the aluminum foam. Due to the stirring during the preparation process, the distribution of BF in aluminum melt is random. Moreover, though the main component of BF is SiO₂, due to the presence of Mg, it has good wettability with aluminum matrix [35]. Thus, the randomly distributed BF mainly constricted in between liquid–gas interfaces during the foaming process, as shown in Figure 7a. In addition, they are more effective at

trapping liquid, thereby improving the stability of the foam. On the other hand, as the bubbles grow up, the liquid film decreases in thickness, liquid–gas interfaces will squeeze BF into a denser structure, and some BF will then partially protrude from the liquid film, as shown in Figure 7c. In addition, when BF is longer than the thickness of the liquid film, it will easily be trapped in the cell walls and will not be able to transfer to the bottom, due to the gravity drainage (Figure 7d) [13,14].

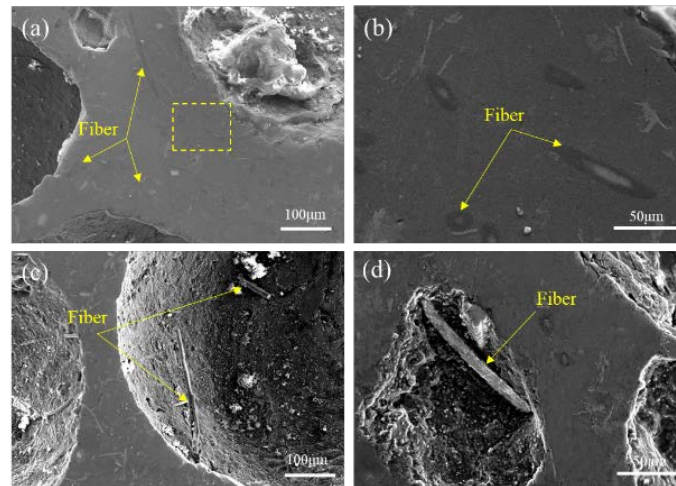


Figure 7. Distribution of BF in the composite foam: (a) Entirely embedded in the cell wall; (b) enlarged image of BF from (a); (c) partially protruding from the cell wall; (d) penetrating through the cell.

To investigate the enhancement mechanism of BF, fracture surfaces of BF-containing foams were observed. Figure 8 shows the failure morphology of the foams with BF completely embedded in the aluminum matrix. As shown in Figure 8a, it breaks simultaneously with the matrix, BF possess optimal compressive strength [15,16], and more energy is required to rupture the cell walls during compression. It has been reported that tensile or shear will occur when forces from other cells are perpendicular to the compression direction [36]. As shown in Figure 8b,c, BF completely embedded in the matrix cracked when subjected to tensile stress. This is because the presence of BF limits the deformation of aluminum matrix, and under tensile stress, BF is subject to greater tensile stress than the matrix [37]. This process plays a key role in dissipating energy. Meanwhile, BF completely embedded in the aluminum matrix enable the cell wall to possess greater compressive stress, leading to the improvement in yield strength. In addition, closed-cell aluminum foam possesses lower thermal conductivity, and during the solidification process, the cooling speed of BF-containing aluminum foam would be different, resulting in casting stress in the foam [15,38]. Besides, average thermal expansion coefficients of BF and pure aluminum are about 7.25×10^{-6} and 24×10^{-6} , respectively, which will also cause residual stress during the preparation process of aluminum foam [39,40]. When the compression stress exceeds the yield strength of BF-containing aluminum foam, it will generate collapse, resulting in a significant stress drop.

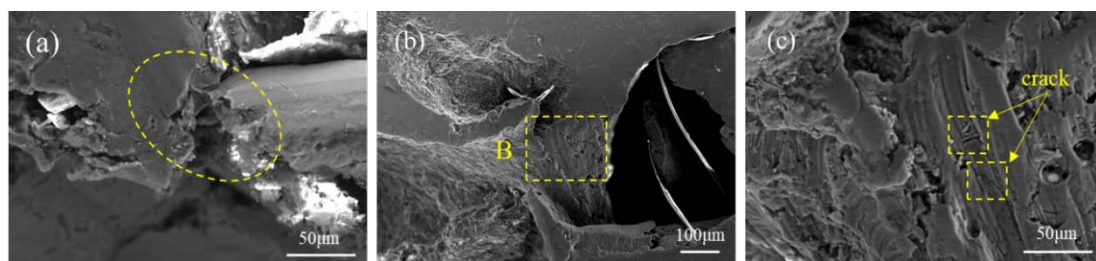


Figure 8. Failure morphology of BF-containing aluminum foam: (a) BF breaking simultaneously with the matrix; (b) necking phenomenon; (c) detail of (B) in (b).

Compression deformation diagrams of BF penetrating through the cell are shown in Figure 9. It can be seen that BF bears both tensile or bend load during the compression process, respectively. Owing to its higher yield strength and tensile strength of BF compared to aluminum matrix, penetrated BF can restrict the deformation of the cell structure and enhance structural stability [15,32]. In addition, friction between BF protruding into the matrix and the matrix will also promote the energy absorption property [41]. Meanwhile, interfacial bonding between BF and the matrix has a critical effect on the mechanical properties of aluminum foam [42,43].

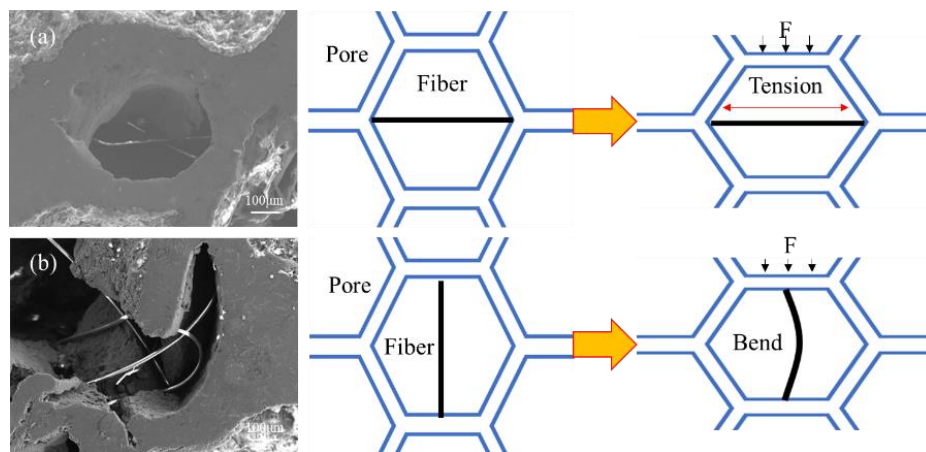


Figure 9. Deformation and load of BF during compression and its schematic diagram: (a) Tensile; (b) bend.

To further investigate the effect of BF on the microstructure of aluminum matrix, SEM analysis was performed along the interface of BF and aluminum matrix (Figure 10). Figure 10b shows line scanning analysis results of a single axially distributed BF and its adjacent aluminum matrix. It can be seen that the intensity of Mg and O is similar with the decrease in aluminum intensity, meaning that there may be a Mg-Al-O enrichment area at the interface. In addition, the intensity of Si fluctuates on the left side of the matrix, meaning that BF may react with the aluminum matrix, leading to Si migrating out of the BF into the matrix [21,37]. Combining with Figure 10a, it can be inferred that strong interface bonding exists between BF and the aluminum matrix. When BF was debonding during compression (Figure 11), more energy will be dissipated.

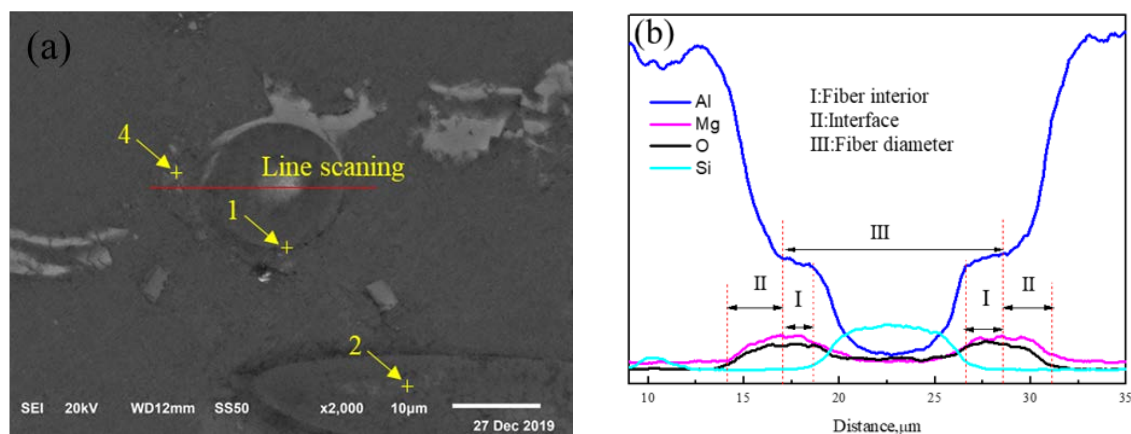


Figure 10. (a) Schematic diagram of line scanning area and (b) results of line scan analysis.

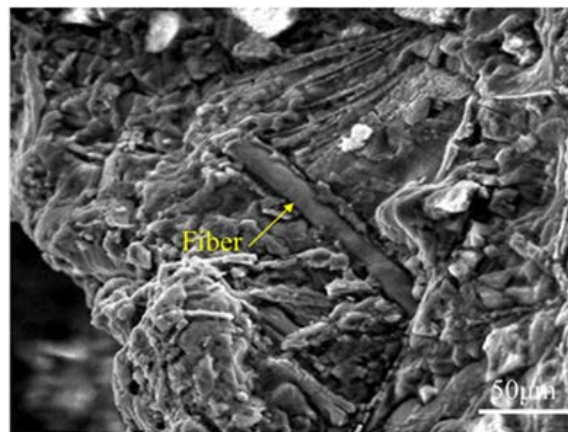


Figure 11. BF exposed in aluminum matrix after compression.

Figure 12 shows surface scanning results of BF-containing aluminum foam. As shown in Figure 12b,d, Mg and O are mainly distributed along BF surfaces. Moreover, a certain amount of Si is distributed in the matrix (Figure 12f), which is consistent with the line scanning results as described above. Furthermore, it is noteworthy that the distribution of Ca in aluminum matrix is similar to that of Si (Figure 12e). Table 1 displays EDX results of different regions in Figures 10a and 12a. It can be seen that the Al/Mg/O ratios are different from different areas. Combined with the line scanning results (Figure 10b), it can be inferred that the BF surface should be coated with a layer of Mg-Al-O intermetallic compounds with its thickness of about 3 μm , which gives further evidence of a good interface combination between BF and aluminum matrix. In addition, according to Al/Ca/Si ratios and surface scanning results in Figure 12, it can also be inferred that the Si diffused into the matrix may form Al-Ca-Si intermetallic compounds with Al and Ca [22]. The presence of these intermetallic compounds can greatly improve the strength of cell walls, thereby improving the mechanical properties of BF-containing aluminum foams.

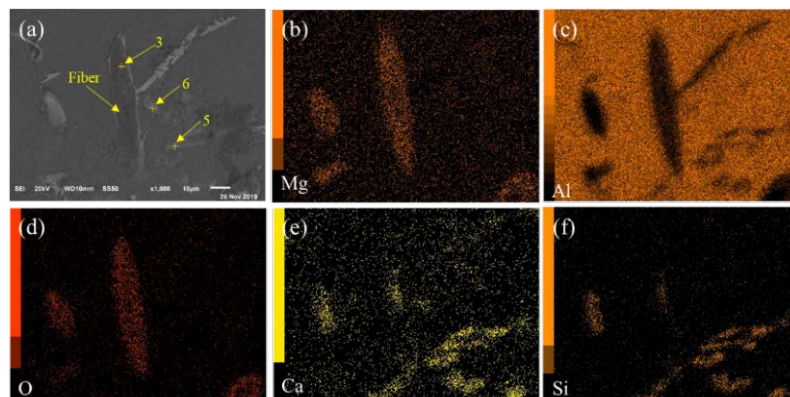


Figure 12. (a) Morphology of BF/Al, and element distribution: (b) Mg; (c) Al; (d) O; (e) Ca; (f) Si.

Table 1. Compositions of different regions.

No.	Composition (wt.%)				
	Al	Mg	O	Si	Ca
1	37.82	10.32	51.58	-	-
2	35.31	11.13	51.38	-	-
3	39.85	10.66	49.32	-	-
4	62.88	-	-	15.98	8.37
5	60.63	-	-	18.54	9.65
6	78.63	-	-	5.69	5.38

5. Conclusions

Closed-cell aluminum foams with 4 wt.% contents of BF were fabricated by the melt-foaming method using Ca, Mg as a thickening agent, and TiH_2 as a foaming agent. The distribution of BF and its effect on the quasi-static compressive properties of closed-cell aluminum foam were investigated, and the following conclusions were obtained: Addition of BF prominently reduced the pore size, enhanced the homogeneity of the pores, and improved the yield strength, plateau stress, and energy absorption capacities of aluminum foams. Compared to pure aluminum foam, the densification strain of BF-containing aluminum foam is insensitive to porosity in the investigated porosity range. In BF-containing aluminum foams, it was observed that some BF embedded entirely in the cell walls, some BF protruded from the cell walls, and some BF penetrated through the cells, and no bundles of BF were found, which is beneficial for the improvement in mechanical properties of BF-containing aluminum foam. Meanwhile, BF has a significant enhancement effect on stabilizing the pore structure and strengthening the matrix. Mg-Al-O and Al-Ca-Si intermetallic compounds formed along the interface of BF and the matrix, respectively. In addition to the traditional way of dissipating energy during the compression process, the fracture of BF, and the debonding and friction of BF/matrix interfaces were also significant for the improvement in energy absorption characteristics.

Author Contributions: Conceptualization, X.C, X.X. and J.D.; data curation, D.Y., X.H., X.X. and Y.W.; formal analysis, D.Y., Z.Z., X.X., X.C., J.D. and H.L.; investigation, D.Y., Z.Z. and T.X.; methodology, X.X., J.D., X.C. and X.L.; writing—Original draft, D.Y., Z.Z. and Y.G.; writing—Review and editing, X.X., J.D., Y.W. and Y.S. All authors have read and agreed to the published version of the manuscript.

Funding: This research was funded by Key R&D Program of Hebei Province (No.19251013D), Special Fund Project for Military-civilian Integration Development of Hebei Province, Provincial School Cooperation Fund of Hebei province, Natural Science Foundation of Hebei Province (No. E2019202161).

Conflicts of Interest: The authors declare no conflict of interest.

References

1. Xia, X.; Chen, X.; Zhang, Z.; Chen, X.; Zhao, W.; Liao, B.; Hur, B. Compressive properties of closed-cell aluminum foams with different contents of ceramic microspheres. *Mater. Des.* **2014**, *56*, 353–358. [[CrossRef](#)]
2. Pinto, S.C.; Marques, P.A.A.P.; Vesenjajk, M.V.; Vicente, R.; Luís, G.; Lovre, K.-O.; Isabel, D. Mechanical, Thermal, and acoustic properties of aluminum foams impregnated with epoxy/graphene oxide nanocomposites. *Metals* **2019**, *9*, 1214. [[CrossRef](#)]
3. Wang, N.Z.; Maire, E.; Chen, X.; Adrien, J.; Li, Y.X.; Amani, Y. Compressive performance and deformation mechanism of the dynamic gas injection aluminum foams. *Mater. Charact.* **2019**, *147*, 11–20. [[CrossRef](#)]
4. Banhart, J. Manufacture, characterisation and application of cellular metals and metal foams. *Prog. Mater. Sci.* **2001**, *46*, 559–632. [[CrossRef](#)]
5. Le Barbenchon, L.; Kopp, J.B.; Girardot, J.; Viot, P. Reinforcement of cellular materials with short fibres: Application to a biobased cork multi-scale foam. *Mech. Mater.* **2020**, *142*, 103271. [[CrossRef](#)]
6. Huang, L.; Wang, H.; Yang, D.H.; Ye, F.; Lu, Z.P. Effects of scandium additions on mechanical properties of cellular Al-based foams. *Intermetallics* **2012**, *28*, 71–76. [[CrossRef](#)]
7. Xia, X.C.; Feng, H.; Zhang, X.; Zhao, W.M. The compressive properties of closed-cell aluminum foams with different Mn additions. *Mater. Des.* **2013**, *51*, 797–802. [[CrossRef](#)]
8. Xia, X.; Zhang, Z.; Wang, J.; Zhang, X.; Zhao, W.; Liao, B.; Hur, B. Compressive characteristics of closed-cell aluminum foams after immersion in simulated seawater. *Mater. Des.* **2015**, *67*, 330–336. [[CrossRef](#)]
9. Orbulov, I.N. Compressive properties of aluminium matrix syntactic foams. *Mater. Sci. Eng. A* **2012**, *555*, 52–56. [[CrossRef](#)]
10. Zhang, Z.; Ding, J.; Xia, X.C.; Sun, X.H.; Song, K.H.; Zhao, W.M.; Liao, B. Fabrication and characterization of closed-cell aluminum foams with different contents of multi-walled carbon nanotubes. *Mater. Des.* **2015**, *88*, 359–365. [[CrossRef](#)]
11. Li, J.; Wu, C.Q.; Hao, H.; Liu, Z.X.; Yang, Y.K. Basalt scale-reinforced aluminum foam under static and dynamic loads. *Compos. Struct.* **2018**, *203*, 599–613. [[CrossRef](#)]

12. Mu, Y.L.; Yao, G.C. Effect of fly ash particles on the compressive properties of closed-cell aluminum foams. *J. Mater. Eng. Perform.* **2010**, *19*, 995–997. [[CrossRef](#)]
13. Mu, Y.L.; Zu, G.Y.; Cao, Z.K.; Yao, G.C.; Wang, Q.D. Metal foam stabilization by copper-coated carbon fibers. *Scr. Mater.* **2013**, *68*, 459–462. [[CrossRef](#)]
14. Cao, Z.K.; Li, B.; Yao, G.C.; Wang, Y. Fabrication of aluminum foam stabilized by copper-coated carbon fibers. *Mater. Sci. Eng. A* **2008**, *486*, 350–356. [[CrossRef](#)]
15. Jamshaid, H. Basalt fiber and its applications. *J. Textile. Eng. Fashion. Technol.* **2017**, *1*, 254–255. [[CrossRef](#)]
16. Fiore, V.; Scalici, T.; Bella, G.D.; Valenza, A. A review on basalt fibre and its composites. *Compos. Part B* **2015**, *74*, 74–94. [[CrossRef](#)]
17. Ward, P.J.; Atkinson, H.V.; Anderson, P.R.G.; Elias, L.G.; Garcia, B.; Kahlen, L.; Rodriguez-Ibabe, J.M. Semi-solid processing of novel MMCs based on hypereutectic aluminium-basal Short fiber alloys. *Acta Mater.* **1996**, *44*, 1717–1727. [[CrossRef](#)]
18. Ezhil, V.S.; Paul, V.S. Microstructure and mechanical properties of as cast aluminium alloy 7075/basalt dispersed metal matrix composites. *J. Miner. Mater. Charact. Eng.* **2014**, *2*, 182–193.
19. Yang, Z.M.; Liu, J.X.; Feng, X.Y.; Xu Li, S.K.; Ren Jie, Y.X. Investigation on mechanical properties and failure mechanisms of basalt fiber reinforced aluminum matrix composites under different loading conditions. *J. Compos. Mater.* **2017**, *52*, 1907–1914.
20. Mc-Danels, D.L. Analysis of Stress-Strain, Fracture, and Ductility Behavior of Aluminum Matrix Composites Containing Discontinuous Basalt Short Fiber Carbide Reinforcement. *Metall. Mater. Trans. A* **1985**, *16*, 1105–1115. [[CrossRef](#)]
21. Akhlaghi, F.; Eslami-Farsani, R.; Sabet, S.M.M. Synthesis and characteristics of continuous basalt fiber reinforced aluminum matrix composites. *J. Compos. Mater.* **2013**, *47*, 3379–3388. [[CrossRef](#)]
22. Adole, O.; Barekar, N.; Anguilano, L.; Minton, T.; Novytskyi, A.; McKay, B. Fibre/matrix intermetallic phase formation in novel aluminium-basalt composites. *Mater. Lett.* **2019**, *239*, 128–131. [[CrossRef](#)]
23. Wang, N.Z.; Chen, X.; Li, Y.X.; Liu, Z.Y.; Zhao, Z.P.; Cheng, Y.; Liu, Y.; Zhang, H.W. The cell size reduction of aluminum foam with dynamic gas injection based on the improved foamable melt. *Colloid. Surface. A* **2017**, *527*, 123–131. [[CrossRef](#)]
24. Yang, K.M.; Yang, X.D.; Liu, E.Z.; Shi, C.S.; Ma, L.Y.; He, C.N.; Li, Q.Y.; Li, J.J.; Zhao, N.Q. Elevated temperature compressive properties and energy absorption response of in-situ grown CNT-reinforced Al composite foams. *Mater. Sci. Eng. A* **2017**, *690*, 294–302. [[CrossRef](#)]
25. Mondal, D.P.; Goel, M.D.; Das, S. Compressive deformation and energy absorption characteristics of closed cell aluminum-fly ash particle composite foam. *Mater. Sci. Eng. A* **2009**, *507*, 102–109. [[CrossRef](#)]
26. Goel, M.D.; Peroni, M.; Solomos, G.; Mondal, D.P.; Matsagar, V.A.; Gupta, A.K.; Larcher, M.; Marburg, S. Dynamic compression behavior of cenosphere aluminum alloy syntactic foam. *Mater. Des.* **2012**, *42*, 418–423. [[CrossRef](#)]
27. Goel, M.D.; Matsagar, V.A.; Gupta, A.K.; Marburg, S. Strain rate sensitivity of closed cell aluminum fly ash foam. *Trans. Nonferrous. Met. Soc.* **2013**, *23*, 1080–1089. [[CrossRef](#)]
28. Zhang, Y.; Jin, T.; Li, S.Q.; Ruan, D.; Wang, Z.H.; Lu, G.X. Sample size effect on the mechanical behavior of aluminum foam. *Int. J. Mech. Sci.* **2019**, *15*, 622–638. [[CrossRef](#)]
29. Wang, Z.H.; Shen, J.H.; Lu, G.X.; Zhao, L.M. Compressive behavior of closed-cell aluminum alloy foams at medium strain rates. *Mater. Sci. Eng. A* **2011**, *528*, 2326–2330. [[CrossRef](#)]
30. Paul, A.; Ramamurty, U. Strain rate sensitivity of a closed-cell aluminum foam. *Mater. Sci. Eng. A* **2000**, *1*, 1–7. [[CrossRef](#)]
31. Su, M.; Wang, H.; Hao, H.; Fiedler, T. Compressive properties of expanded glass and alumina hollowspheres hybrid reinforced aluminum matrix syntactic foams. *J. Alloys Compd.* **2020**, *821*, 153233. [[CrossRef](#)]
32. Xie, B.; Fan, Y.Z.; Mu, T.Z.; Deng, B. Fabrication and energy absorption properties of titanium foam with CaCl₂ as a space holder. *Mater. Sci. Eng. A* **2017**, *708*, 419–423. [[CrossRef](#)]
33. Liu, J.A.; Yu, S.R.; Hu, Z.Q.; Liu, Y.H.; Zhu, X.Y. Deformation and energy absorption characteristic of Al₂O₃/Zn–Al composite foams during compression. *J. Alloys Compd.* **2010**, *506*, 620–625. [[CrossRef](#)]
34. Mu, Y.L.; Yao, G.C.; Cao, Z.K.; Luo, H.J.; Zu, G.Y. Strain-rate effects on the compressive response of closed-cell copper-coated carbon fiber/aluminum composite foam. *Scr. Mater.* **2011**, *64*, 61–64. [[CrossRef](#)]

35. Lin, Y.F.; Zhang, Q.; Chang, J.; Wang, H.Y.; Feng, X.W.; Wang, J. Microstructural characterization and compression mechanical response of glass hollow spheres/Al syntactic foams with different Mg additions. *Mater. Sci. Eng. A* **2019**, *766*, 138338. [[CrossRef](#)]
36. Kadkhodapour, J.; Raeisi, S. Micro–macro investigation of deformation and failure in closed-cell aluminum foams. *Comp. Mater. Sci.* **2014**, *83*, 137–148. [[CrossRef](#)]
37. Kannan, K.; Misra, A. Short glass fiber reinforced PA6 and ABS blends: Mechanical properties and morpholog. *Int. Polym. Process.* **1994**, *9*, 184–192. [[CrossRef](#)]
38. Xia, X.C.; Zhao, W.M.; Feng, X.Z.; Feng, H.; Zhang, X. Effect of homogenizing heat treatment on the compressive properties of closed-cell Mg alloy foams. *Mater. Des.* **2013**, *49*, 19–24. [[CrossRef](#)]
39. Jiang, Z.H.; Lian, J.S.; Yang, D.Z.; Dong, S.L. An analytical study of the influence of thermal residual stresses on the elastic and yield behaviors of short fiber-reinforced metal matrix composites. *Mater. Sci. Eng. A* **1998**, *248*, 256–275. [[CrossRef](#)]
40. Ezhil Vannana, S.; Paul Vizhian, S.; Karthigeyan, R. Investigation on the influence of basalt fiber on thermal properties of Al7075/ basalt fiber metal matrix composites. *Procedia Eng.* **2014**, *97*, 432–438. [[CrossRef](#)]
41. Noda, N.A.; Chen, D.; Zhang, G.W.; Sano, Y. Single-fiber pull-out analysis comparing the intensities of singular stress fields (ISSFs) at fiber end/entry points. *Int. J. Mech. Sci.* **2020**, *165*, 105196. [[CrossRef](#)]
42. Aghamohammadi, H.; Abbandanak, S.N.; Eslami-Farsani, R.; Siadati, S.H. Effects of various aluminum surface treatments on the basalt fiber metal laminates interlaminar adhesion. *Int. J. Adhes. Adhes.* **2018**, *84*, 184–193. [[CrossRef](#)]
43. Yua, S.; Oh, K.H.; Hong, S.H. Enhancement of the mechanical properties of basalt fiber-reinforced polyamide 6,6 composites by improving interfacial bonding strength through plasma-polymerization. *Compos. Sci. Technol.* **2019**, *182*, 107756. [[CrossRef](#)]



© 2020 by the authors. Licensee MDPI, Basel, Switzerland. This article is an open access article distributed under the terms and conditions of the Creative Commons Attribution (CC BY) license (<http://creativecommons.org/licenses/by/4.0/>).